VNU Journal of Science: Mathematics – Physics, Vol. 39, No. 1 (2023) 13-26

VNU Journal of Science: Mathematics - Physics

Journal homepage: https://js.vnu.edu.vn/MaP

Original Article

The Contribution of Photon, Z Boson, Higgs, Radion and Unparticle to the Process $\mu^+\mu^- \to \mu^+\mu^-$ in Randall-Sundrum model

Le Mai Dung*, Dao Thi Le Thuy

Hanoi National University of Education, 136 Xuan Thuy, Cau Giay, Hanoi, Vietnam

Received 23 August 2022
Revised 25 October 2022; Accepted 18 November 2022

Abstract: The process $\mu^+\mu^- \to \mu^+\mu^-$ is studied from unparticle physics perspective in Randall-Sundrum model. We calculated and evaluated the cross sections independently for photon (γ), Z boson (Z), vector unparticle (U^μ), Higgs (h), radion (ϕ), scalar unparticle (U) exchange. Numerical calculations showed that the contribution of unparticle exchange dominates in a very high energy region. While γ and Z contribute mainly in the lower region, h and ϕ contribution is negligible in comparison with the other exchanges. The results are plotted in the energy ranges available in the present designs of accelerators and near future high energy frontier muon colliders as shown by International Muon Collider Collaboration articles.

Keywords: Muon production, unparticle physics, $\mu^+\mu^-$ collisions, muon colliders, Randall-Sundrum model.

1. Introduction

It is renowned that the conformal symmetry plays a pivotal role in both the field theory, theory of superstring and the critical phenomena. In particle physics in four dimensional spacetime, however, the symmetry is broken by the masses of particles. Furthermore, conformal symmetry exists classically and also broken by the effect of renormalization. At the high energy scale, there might be fields with nontrivial scale invariance, such as the Banks-Zaks field [1], which is suggested by Georgi [2] as scale

* Corresponding author.
E-mail address: thuydtl@hnue.edu.vn

https//doi.org/10.25073/2588-1124/vnumap.4755

invariant stuff or unparticles. The existence of unparticles is considered a component of the Beyond Standard Model (BSM) physics above the TeV scale. The theories with nontrivial infrared fix point is sophisticated, Georgi has used the method of the low effect field theory to study unparticles production [2] and unusual virtual effects in high energy processes [3]. The very high energy theory contains the SM field and Banks-Zaks (*BZ*) fields with a nontrivial infrared fixed point. The operators O_{BZ} made of *BZ* fields interacting with the operators O_{SM} built out of SM fields through the exchange of particles with a large mass M_U, which has the following form:

$$\frac{1}{M_U^{d_{SM}+d_{BZ}-4}} O_{SM} O_{BZ} \tag{1}$$

where d_{SM} and d_{BZ} are mass dimensions of *SM* and *BZ* fields, respectively. The *BZ* operators match onto the unparticle operators O_U below the energy Λ_U because of dimensional transmutation from renormalization effects in the *BZ* sector [4], then (1) will have a form:

$$C_{O_U} \frac{\Lambda_U^{d_{BZ}-d_U}}{M_U^{d_{SM}+d_{BZ}-4}} O_{SM} O_U \tag{2}$$

where d_U is the scaling dimension of the unparticle operator O_U and the constant C_{O_U} is a coefficient function fixed by the matching condition. In this work, we will restrict ourselves to the scalar and vector unparticle operators as propagators in $\mu^+\mu^-$ process which transforms under the standard model gauge group as a standard model singlet [5, 6]. From the effective interactions satisfying the gauge symmetry for the scalar and vector unparticle operators with SM fields in [5], we will have Feynman rules as follows:

$$\begin{gathered} i\frac{\lambda_0}{\Lambda_U^{d_U-1}},\ \frac{-\lambda_0}{\Lambda_U^{d_U-1}}\gamma^5,\ \frac{\lambda_0}{\Lambda_U^{d_U}}\not{p},\ 4i\frac{\lambda_0}{\Lambda_U^{d_U}}\left(-p_1.p_2 g^{\mu\nu}+p_1^{\nu}p_2^{\mu}\right) \\ i\frac{\lambda_1}{\Lambda_U^{d_U-1}}\gamma^{\mu},\ i\frac{\lambda_1}{\Lambda_U^{d_U-1}}\gamma^{\mu}\gamma^5 \end{gathered} \tag{3}$$

where λ_i are dimensionless effective couplings $(C_{O_U^i}\Lambda_U^{d_{BZ}})/M_U^{d_{SM}+d_{BZ}-4}$ from the form (2) with the index i = 0, 1 or 2 corresponding to the scalar, vector and tensor unparticle operators, respectively.

The unparticle propagators have the form

$$\begin{aligned} \Delta_{scalar}(q^2) &= \frac{A_{d_U}}{2\sin(d_U\pi)}(-q^2)^{d_U-2} \\ \Delta_{vector}(q^2)_{\mu\nu} &= \frac{A_{d_U}}{2\sin(d_U\pi)}(-q^2)^{d_U-2}\pi_{\mu\nu}(q) \end{aligned} \tag{4}$$

where

$$A_{d_U} = \frac{16\pi^2\sqrt{\pi}}{(2\pi)^{2d_U}}\frac{\Gamma(d_U+1/2)}{\Gamma(d_U-1)\Gamma(2d_U)},\ \pi_{\mu\nu}(q) = -g_{\mu\nu}+\frac{q_\mu q_\nu}{q^2} \tag{5}$$

$(-q^2)$ is defined as follows, it is positive in t- and u-channel, but negative in s-channel process

$$(-q^2)=\begin{cases}\left|q^2\right|^{d_U-2} & q^2<0\\ \left|q^2\right|^{d_U-2}e^{-id_U\pi} & q^2>0\end{cases} \tag{6}$$

Even though the undoubted success of the SM, it still has problems in terms of theoretical aspects. The need of new physics has become urgent as there have been several problems relating to the gauge hierarchy between the Planck scale and the weak one. The SM evidently offers no explanation of mass hierarchy, of dark matter, of the baryon asymmetry, etc. In due course, many attempts and theories are proposed to solve the problems, yet the Randall-Sundrum (RS) model is one of the most prosperous extensions to be existed. The RS model was formulated by Randall and Sundrum [7], who hypothesize a five-dimensional universe with two four dimensional surfaces called 3-branes. All the SM particles and forces are assumed to be confined to the IR brane, the gravity lives on the UV brane and in the bulk. The model is defined by the five-dimensional action

$$S=-\int d^4xdy\sqrt{-\hat{g}}\left(\frac{R}{16\pi G_5}+\Lambda\right)+\int d^4x\sqrt{-g_{hid}(L_{hid}-V_{hid})}+\int d^4x\sqrt{-g_{vis}(L_{vis}-V_{vis})} \tag{7}$$

where $\hat{g}^{\hat{\mu}\hat{\nu}}(\hat{\mu},\hat{\nu}=0,1,2,3,4,$ where 4 refers to the coordinate y) is the bulk metric, $g_{hid}^{\mu\nu}\equiv\hat{g}^{\mu\nu}(x,y=0)$ and $g_{vis}^{\mu\nu}\equiv\hat{g}^{\mu\nu}(x,y=1/2)$ are the induced metrics on the branes. If the boundary conditions are periodic and the bulk and brane cosmological constants satisfying this relation $\Lambda/m_0=-V_{hid}=V_{vis}=-12m_0/\varepsilon^2$. We will have the background metric of the RS1 model

$$ds^2=e^{-2\sigma(y)}\eta_{\mu\nu}dx^\mu dx^\nu-b_0^2dy^2 \tag{8}$$

where $\sigma(y)=m_0b_0[y(2\theta(y)-1)-2(y-1/2)\theta(y-1/2)]$, b_0 is a constant parameter is not determined by the five-dimensional action. Gravitational fluctuations around the metric will be defined through the following replacements

$$\eta_{\mu\nu}\to\eta_{\mu\nu}+\varepsilon h_{\mu\nu}(x,y);\;\; b_0\to b_0+b(x) \tag{9}$$

In the RS model, the bare parameters are valued by the Planck scale. The applicable value for size of the extra dimension is adjusted by $kr_c\pi\simeq 35$ (r_C is the compactification radius and k is the bulk curvature). Therefore, the weak and gravity scales are generated in a natural way. The mixing of gravity and scalar has the following form

$$S_\xi=-\xi\int d^4x\sqrt{g_{vis}}R(g_{vis})\hat{H}^\dagger\hat{H} \tag{10}$$

where ξ is the dimensionless mixing parameter, $R(g_{vis})$ is the Ricci scalar for the metric $g_{vis}^{\mu\nu}=\Omega_b^2(x)(\eta^{\mu\nu}+\varepsilon h^{\mu\nu})$ induced on the visible brane. $\Omega_b(x)=e^{-kr_C\pi}(1+\phi_0/\Lambda_\phi)$ is the warp factor, ϕ_0 is the normalized massless radion field, H is the Higgs field in the five dimensional universe before rescaling on the brane. The mixing term mixes the h_0 and ϕ_0 into the mass eigenstates h and ϕ

$$\begin{pmatrix}h_0\\ \phi_0\end{pmatrix}=\begin{pmatrix}1 & -6\xi\gamma/Z\\ 0 & 1/Z\end{pmatrix}\begin{pmatrix}\cos\theta & \sin\theta\\ -\sin\theta & \cos\theta\end{pmatrix}\begin{pmatrix}h\\ \phi\end{pmatrix}=\begin{pmatrix}d & c\\ b & a\end{pmatrix}\begin{pmatrix}h\\ \phi\end{pmatrix} \tag{11}$$

where

$$\gamma \equiv \frac{v_0}{\Lambda_\phi},\ Z = \sqrt{\beta - 36\xi^2\gamma^2},\ \beta = 1 - 6\xi\gamma^2,$$
$$a = \frac{\cos\theta}{Z},\ b = -\frac{\sin\theta}{Z},\ c = \sin\theta - \frac{6\xi\gamma}{Z}\cos\theta,\ d = \cos\theta + \frac{6\xi\gamma}{Z}\sin\theta \tag{12}$$

The mixing angle is given by

$$\tan 2\theta = 12\gamma\xi Z \frac{m_{h_0}^2}{m_{h_0}^2(Z^2 - 36\xi^2\gamma^2) - m_{\phi_0}^2} \tag{13}$$

Subsequently, the new physical field *h* and ϕ are Higgs-dominated state and radion with the mass

$$m_{h,\phi}^2 = \frac{1}{2Z^2}\left[m_{\phi_0}^2 + \beta m_{h_0}^2 \pm \sqrt{(m_{\phi_0}^2 + \beta m_{h_0}^2)^2 - 4Z^2 m_{\phi_0}^2 m_{h_0}^2} \right] \tag{14}$$

A review of muon physics and up-to-date colliders experiments – Regarding the muon process, muons could be accelerated and interact in the collider rings without suffering from the great synchrotron radiation losses that presently restrain the performance of electron-positron colliders. The proposal of muon colliders has received huge interests from the particle physics community in recent years on account of its potential of reaching very high energies in a compact tunnel at comparatively low expense. It has also been argued that the discovery probability of certain processes or heavy particles at a 14 TeV muon collider matches that at a 100 TeV *pp* (proton-proton) collider namely Future Circular Collider (FCC-hh) [8, 9] when the available beam energy is carried by muon particles. A muon collider is expected to be one of the most energy efficient selections for the exploration of new physics in the energy frontier from 2 TeV to approximately 10 TeV [10]. For the first time, unstable particles have been deployed in a collider.

In principle, the new energy frontiers colliders with more complex structures of magnets and more advanced and longer tunnels, then the expense is also a great concern. Exploring the feasibility of collider technology and building new accelerator not just provide better alternatives but will be transformative in bringing the field of particle physics, high energy physics and nuclear physics closer to the new energy regions.

2. Calculation

Applying the Feynman rules and effective interactions, one can have diagrams shown in Fig. 1.

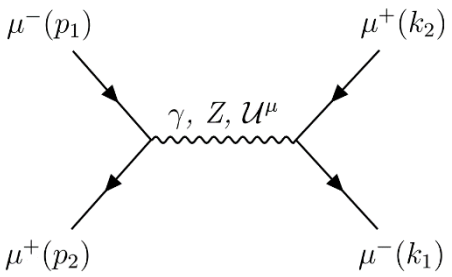

s-channel

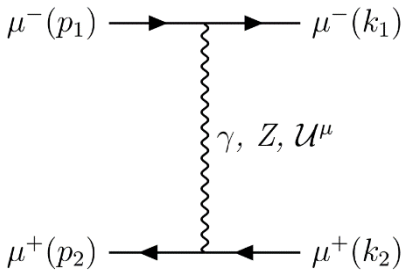

u-channel

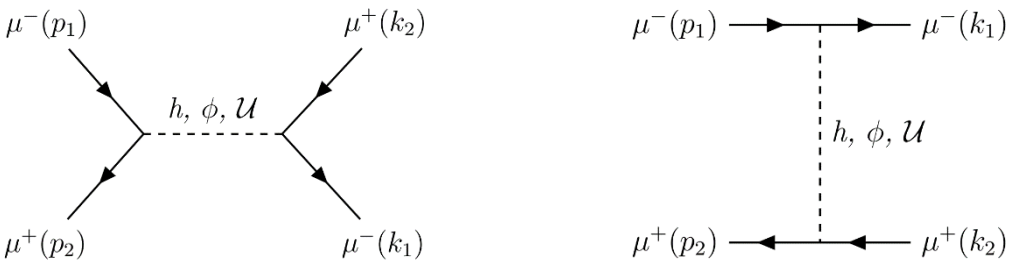

s-channel u-channel

Figure 1. Feynman diagrams of the process $\mu^+\mu^- \to \mu^+\mu^-$.

We consider the two following processes in which the initial state of muon beams are unpolarized. The propagating contributions are γ , *Z*, h, ϕ , scalar and vector unparticles *U* and U^μ.

$$\begin{aligned} &\mu^+\mu^- \underline{\gamma, Z, U^\mu} \mu^+\mu^- \\ &\mu^+\mu^- \underline{h, \phi, U} \mu^+\mu^- \end{aligned} \tag{15}$$

The transition amplitudes are given by

via (γ , *Z*, U^μ) exchange

$$M_\gamma = \frac{im_\mu^2}{q^2}\bar{v}(p_2)\gamma_\mu u(p_1)\bar{u}(k_1)\gamma^\mu v(k_2) \tag{16}$$

$$\begin{aligned} M_Z = &\left(\frac{g}{4\cos\theta_W}\right)^2 \frac{i}{q^2 - m_Z^2}\left[g_{\mu\nu} - \frac{q_\mu q_\nu}{m_Z^2}\right]\bar{v}(p_2)\gamma^\nu[(1-4s_W^2)+\gamma_5]u(p_1) \\ &\times \bar{u}(k_1)\gamma^\mu[(1-4s_W^2)+\gamma_5]v(k_2) \end{aligned} \tag{17}$$

$$\begin{aligned} M_{U^\mu} = &-\left(\frac{\lambda_1}{\Lambda_U^{d_U-1}}\right)^2 \left(\frac{A_{d_U}\left(-q^2\right)^{d_U-2}}{2\sin\left(d_U\pi\right)}\right)\left[-g_{\mu\nu} + \frac{q_\mu q_\nu}{q^2}\right]\bar{v}(p_2)\gamma^\nu\left(1+\gamma_5\right)u(p_1) \\ &\times \bar{u}(k_1)\gamma^\mu(1+\gamma_5)v(k_2) \end{aligned} \tag{18}$$

via (h, ϕ , *U*) exchange

$$M_h = -i\left(\frac{g}{2}\left[\frac{m_e}{m_W}\left(d + \gamma b\right)\right]\right)^2 \frac{1}{q^2 - m_h^2}\bar{v}\left(p_2\right)u\left(p_1\right)\bar{u}\left(k_1\right)v\left(k_2\right) \tag{19}$$

$$M_\phi = -i\left(\frac{g}{2}\left[\frac{m_e}{m_W}\left(c + \gamma a\right)\right]\right)^2 \frac{1}{q^2 - m_\phi^2}\bar{v}\left(p_2\right)u\left(p_1\right)\bar{u}\left(k_1\right)v\left(k_2\right) \tag{20}$$

$$M_U = -\left(\frac{\lambda_0}{\Lambda_U^{d_U-1}}\right)^2 \left(\frac{A_{d_U}\left(-q^2\right)^{d_U-2}}{2\sin\left(d_U\pi\right)}\right)\bar{v}\left(p_2\right)\left(1 + i\gamma_5 - \frac{i\not{q}}{\Lambda_U}\right)u\left(p_1\right)\bar{u}\left(k_1\right)\left(1 + i\gamma_5 - \frac{i\not{q}}{\Lambda_U}\right)v\left(k_2\right) \tag{21}$$

where $q = p_1 + p_2 = k_1 + k_2$.

By using these transition amplitudes, we evaluate the differential cross section of the process by the expression $\frac{d\sigma}{d\cos\theta} = \frac{1}{128\pi s}\left|\frac{\vec{k_1}}{\vec{p_1}}\right|\left|M_{fi}\right|^2$ [11], where M_{fi} is the transition amplitude, $s = (p_1 + p_2)^2$ and θ is the scattering angle between $\vec{p_1}$ and $\vec{k_1}$.

3. Results and Discussion

For numerical calculations, the primary parameters are chosen as follows: the vacuum expectation of the radion field is $\Lambda_\phi = 5$ TeV [12], the radion mass has been chosen $m_\phi = 10$ GeV [13], the Higgs mass $m_h = 125$ GeV, the mixing parameter $\xi = 1/6$. The parameters of unparticle are selected: $\Lambda_U = 1000$ GeV, $\lambda_0 = \lambda_1 = 1$ and d_U = 1.7.

In the next part of this section, the differential cross sections (DCS) versus the cosine function of scattering are plotted. In Fig. 2a and 2b, the DCS of the final state in s-channel reaches a maximum of 7.24 fb as cosθ equals to ±1, even so the final state in t-channel is observed with higher values as cosθ rises above 0.5. More noticeably, Z exchange of the process in s-channel is small in comparison with the two exchanges γ and U^μ in s-channel and the DCS for Z exchange in t-channel has a large value of 0.27×10^6 fb when cosθ is nearly 0.855. The value of DCS for vector unparticle has a considerable rise as cosθ ranges around 0.5-1, significantly larger than the contribution of γ exchange in t-channel.

There are the same patterns of (h, ϕ) exchange or Higgs-radion propagator when it comes to the scattering angle and the DCS values, thus far the contribution from ϕ exchange in both channels is evidently negligible. Regarding (h, ϕ) exchange, the DCSs decline from the maxima as cosθ runs from –1 to 1 (in Fig. 3a and 3b). The effect of scalar unparticle propagator has greater impact on the observation of the final state rather than the Higgs-radion effect. In Fig. 3c, the DCS decreases significantly from the largest value of 5.82×10^5 fb in the whole process when compared to the other exchanges. The figure decreases to 0 when cosθ ranges from –1 to 1. The DCS figures for (h, ϕ, U) exchange in s-channel are not dependent on the scattering angle, the DCS figures are 4×10^{-2} fb, 4×10^{-16} fb, 0.6×10^5 fb respectively. In t-channel, when cosθ is –1, we have three largest figures, 3.65×10^{-12} fb, 3.69497×10^{-25} fb, 5.8×10^5 fb for each exchange (h, ϕ, U).

To put in a nutshell, the DCS in the two mentioned processes via (γ, Z, U^μ) and (h, ϕ, U) exchange varies greatly in two channels, especially in terms of the range of value. Figure 1 shows that the contribution from (γ, Z, U^μ) exchange is distributed rather consistently, which is different from the three exchanges (h, ϕ, U) when the major contribution coming from scalar unparticles.

In the rest of this section, we plot the total cross sections (TCS) as functions of the collision energy $\sqrt{s}$ via (γ, Z, U^μ) and (h, ϕ, U) exchange in s-channel and t-channel. The collision energy ranges from 100 GeV to 3 TeV, which seems applicable and probable for the present colliders namely CLIC, and near future muon colliders [14-16].

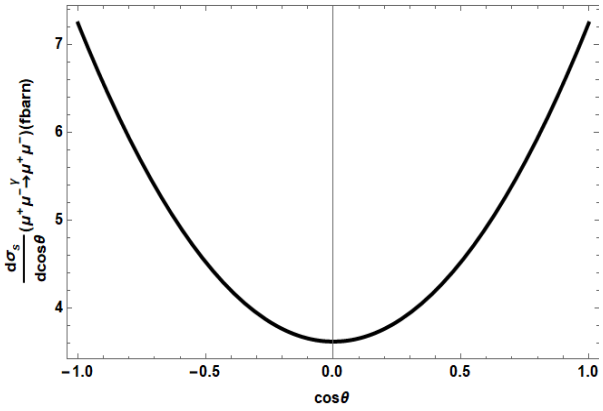

(a) γ exchange in s-channel

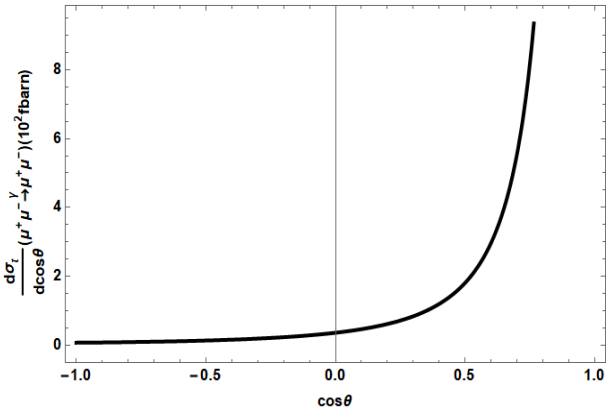

(b) γ exchange in t-channel

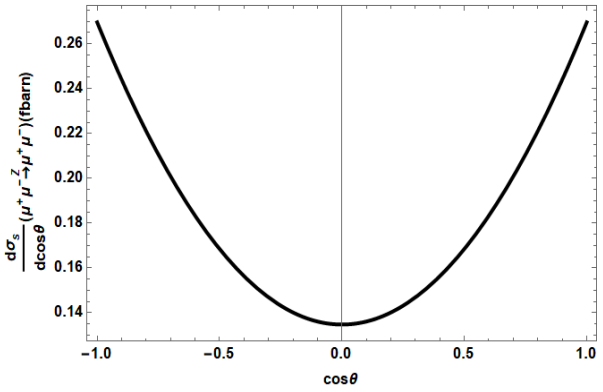

(c) Z exchange in s-channel

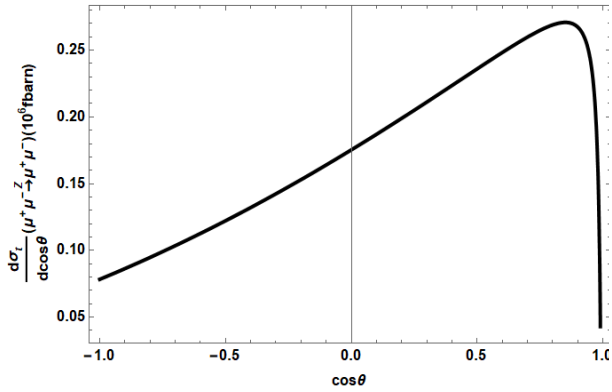

(d) Z exchange in t-channel

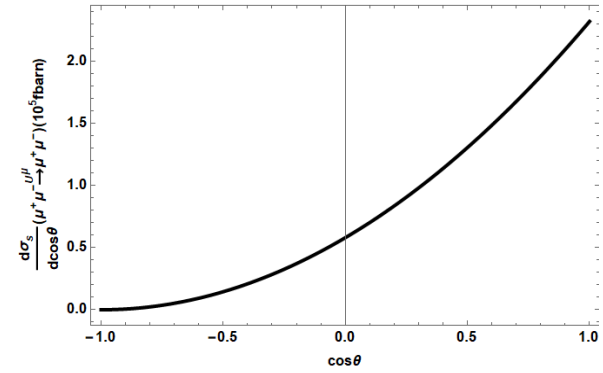

(e) U^μ exchange in s-channel

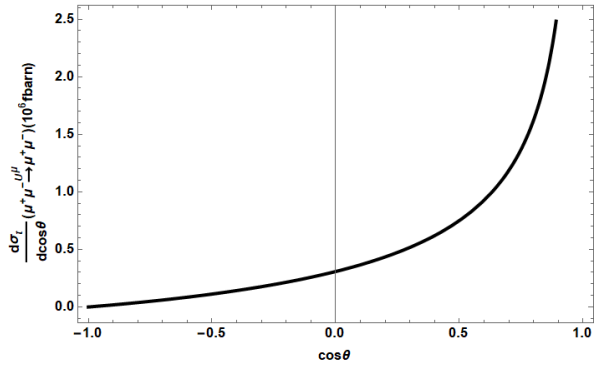

(f) U^μ exchange in t-channel

Figure 2. Differential cross sections as functions of $\cos\theta$ through s-, t- channel with γ , Z, U^μ exchange.

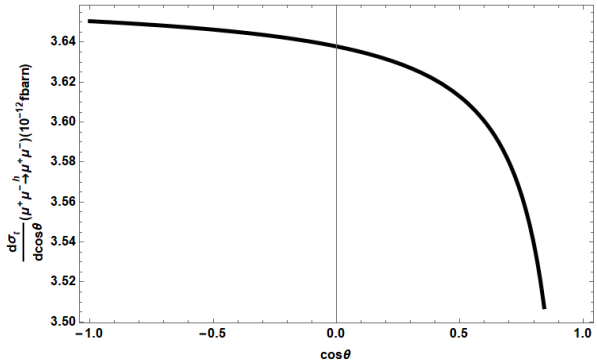

(a) *h* exchange in t-channel

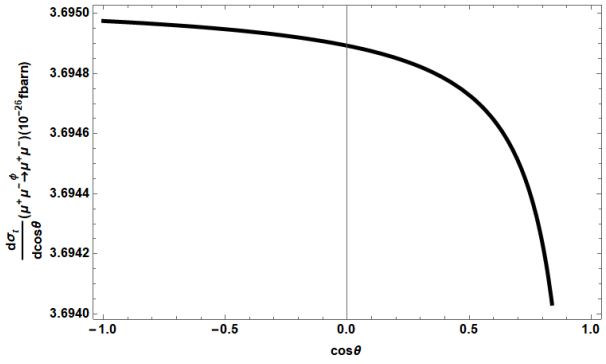

(b) ϕ exchange t-channel

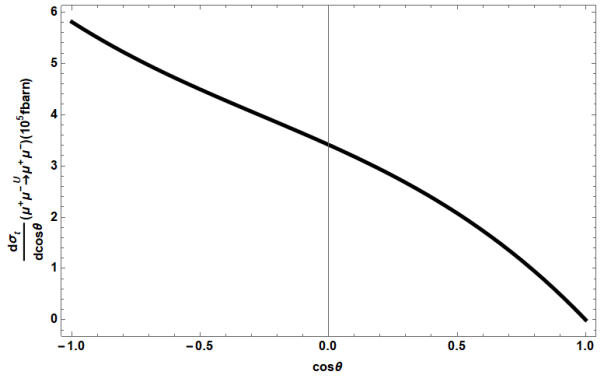

(f) *U* exchange in t-channel

Figure 3. Differential cross sections as functions of $\cos\theta$ through s-, t- channel with h, ϕ , *U* exchange.

The TCS via γ exchange decreases rapidly as the energy reaches 3 TeV, especially TCS in s-channel, only around 0.4-1 TeV (Fig. 4a). Overall, the cross sections achieve the maxima region when the collision energy is below 1.5-2 TeV, for the rest of the higher energy region above 2 TeV, it stays flat (Fig. 6a).

In Fig. 4b, the different patterns in t-channel can be seen when the TCS via *Z* exchange rises considerably following the increase of the collision energy. Meanwhile, the TCS in s-channel appears to reach the bottom steeply and marginally increases as over 2 TeV threshold (Fig. 6c).

Prominently, U^{μ} exchange contribution in the process is tremendous especially in the 1.5-3 TeV, t-channel becomes more effective to observe the final state $\mu^+\mu^-$ via vector unparticles. As the results of the DCS in the previous part of the section, in general, the effect of unparticle propagator is clearly substantial in two channels, with an emphatic in t-channel figure (in Figs. 6e and 6f).

To sum up, via (γ , *Z*, U^{μ}) exchange, the TCS in t-channel will give the most evident observation due to the rapid change over a wide range of higher collision energies. More importantly, the contributions of *Z* boson and vector unparticles are great and easily recognizable, especially for the observation at very high energy, contrasting with the high value of TCS as for γ exchange in lower energy region.

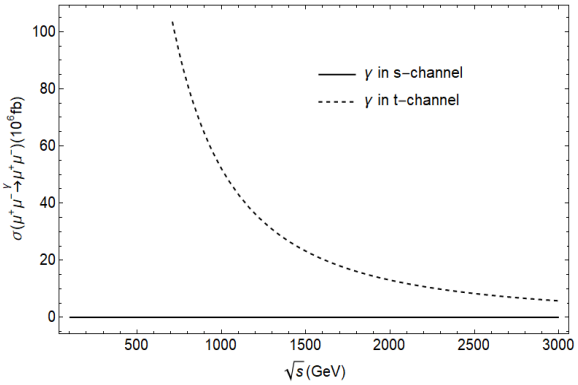

(a) Total cross sections as functions of the center-of-mass energy via γ exchange in s- and t- channel.

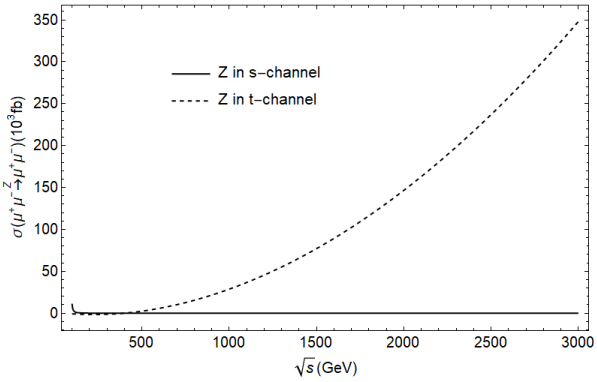

(b) Total cross sections as functions of the center-of-mass energy via Z exchange in s- and t- channel.

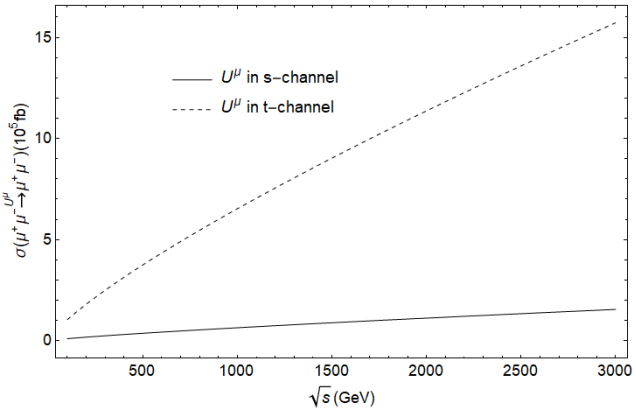

(c) Total cross sections as functions of the center-of-mass energy via U^{μ} exchange in s- and t- channel.

Figure 4. Total cross sections as functions of the center-of-mass energy via (γ , Z, U^{μ}) exchange.

Concerning the three exchanges (h, ϕ , U), in Fig. 5a the TCS via Higgs exchange is infinitesimal (around 10^{-10} fb). The figure declines significantly when the energy reaches higher region above 1.5-2 TeV, but in the lower energy range below 1 TeV, the figure in t-channel has a larger drop.

Interestingly, the TCSs via ϕ exchange in channel s and t are extremely small and different in values leading to the closeness of both TCSs (Fig. 5b). Yet we might recognize very small changes in both TCS values if it is displayed in a higher quality figure (Fig. 7c and 7d). The TCS all decrease rapidly around the 0.5-1 TeV region.

The TCSs via U exchange increase rapidly in the high energy range (Fig. 5c); therein, the figure in t-channel rises more exponentially than in s-channel (Fig. 7e and 7f), and even reach larger value of more than 6×10^5 fb, the largest value for the TCS through both channels via every exchange.

Two important points to be mentioned here are the strong unparticle effect on the final state observation via three exchanges (h, ϕ , U). The other point is that the energy regions chosen to make an

observing scheme, for Higgs-radion, it should be lower in the colliders, the high end should be for the scalar unparticles.

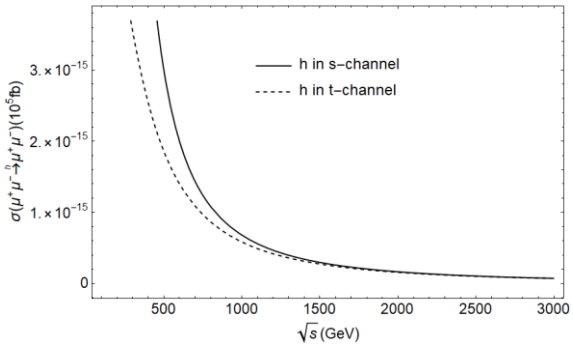

(a) Total cross sections as functions of the center-of-mass energy via *h* exchange in s- and t- channel.

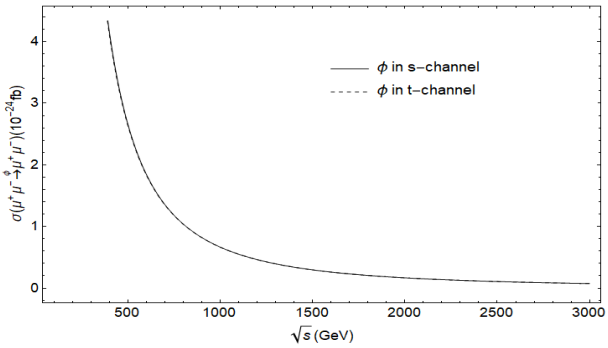

(b) Total cross sections as functions of the center-of-mass energy via ϕ exchange in s- and t- channel.

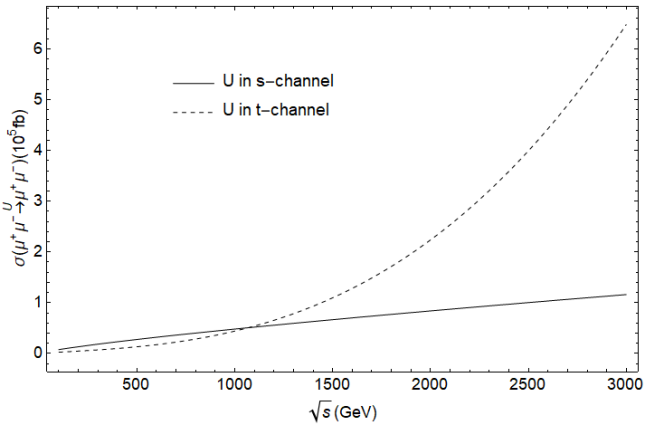

(c) Total cross sections as functions of the center-of-mass energy via *U* exchange in s- and t- channel.

Figure 5. Total cross sections as functions of the center-of-mass energy via (h, ϕ , *U*) exchange.

In this part, we concentrated on total cross sections versus $\sqrt{s}$ in the appropriate energy range. The energy reach we put a limit in the article is possible at the present and near future energy frontiers muon colliders, namely 4 TeV muon collider FNAL Fermilab, a pulsed 14 TeV $\mu^+\mu^-$ collider in the LHC tunnel at CERN [17, 18]. Apart from standard model particles contribution, the outstanding contribution of unparticles and Z boson in high energy region adds up the figure of DCS and TCS, leading to the more accurate measurements. Taking unparticle physics into account, its effect will be more of physical significance. New physics, however, experimentally, will not be effortless to be observed separately in high energy experiments as the concurrence of many models therein a huge amount of hidden and secondary processes emerge. In the matter of the process $\mu^+\mu^- \to \mu^+\mu^-$, through the exchanges of photon, Higgs-radion, vector unparticles and scalar unparticles, we provide the calculation of these particles exchange for the experimental cross-section. Under the case of this model with new particles participation, those possibly contribute to some extent to the cross-sections results. That contribution

consequently increases the cross-section which, no doubt, is not able to be separated with respect to each of new particle exchanges.

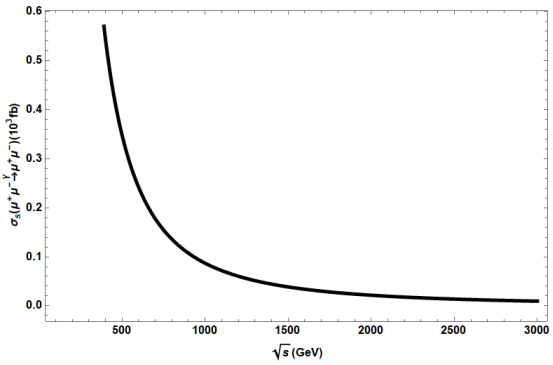

(a) Total cross section as functions of the collision energy via γ exchange in s-channel.

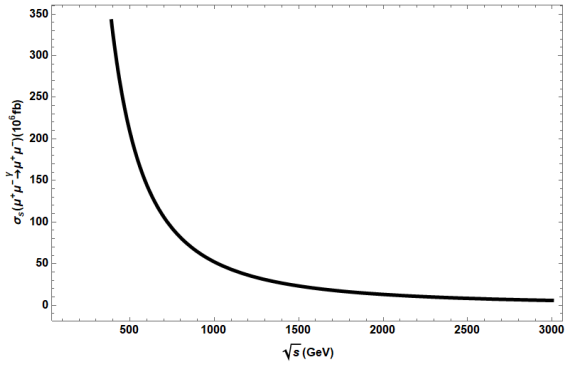

(b) Total cross section as functions of the collision energy via γ exchange in t-channel.

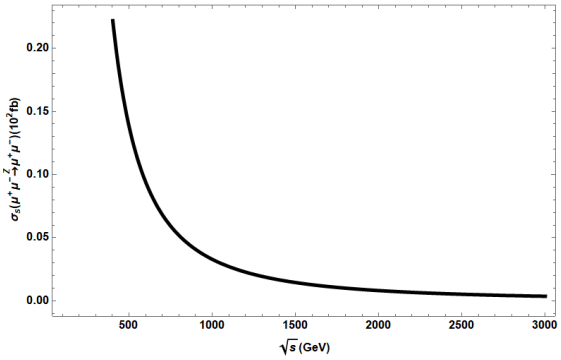

(c) Total cross section as functions of the collision energy via Z exchange in s-channel.

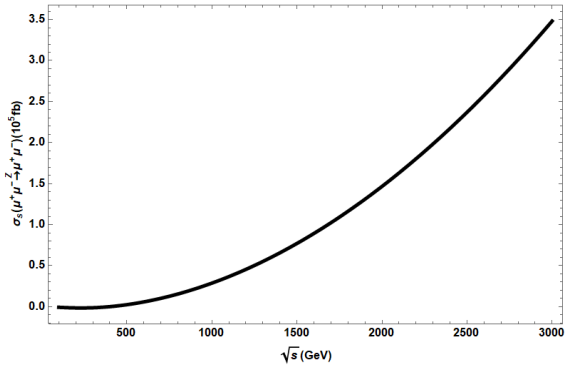

(d) Total cross section as functions of the collision energy via Z exchange in t-channel.

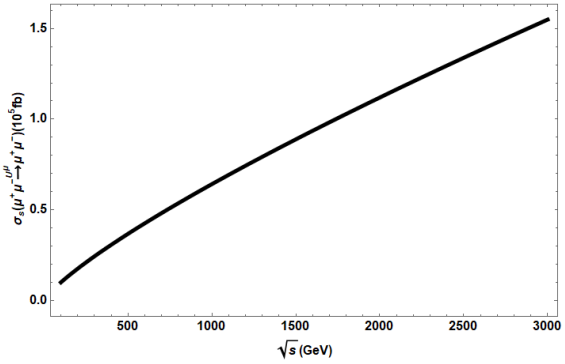

(e) Total cross section as functions of the collision energy via U^{μ} exchange in s-channel.

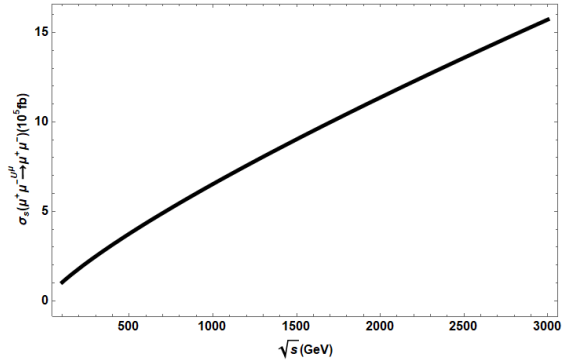

(f) Total cross section as functions of the collision energy via U^{μ} exchange in t-channel.

Figure 6. Total cross sections as functions of the center-of-mass energy via (γ, Z, U^{μ}) exchange through two channels s and t.

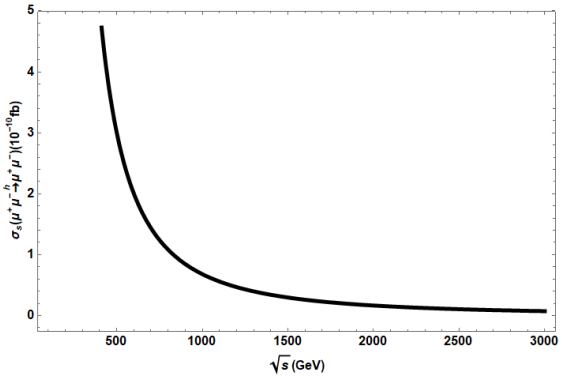

(a) Total cross section as functions of the collision energy via h exchange in s-channel.

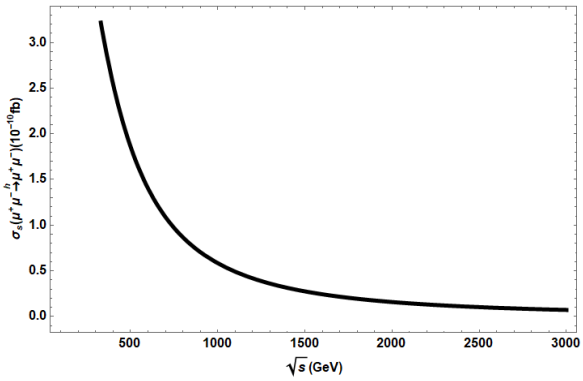

(b) Total cross section as functions of the collision energy via h exchange in t-channel.

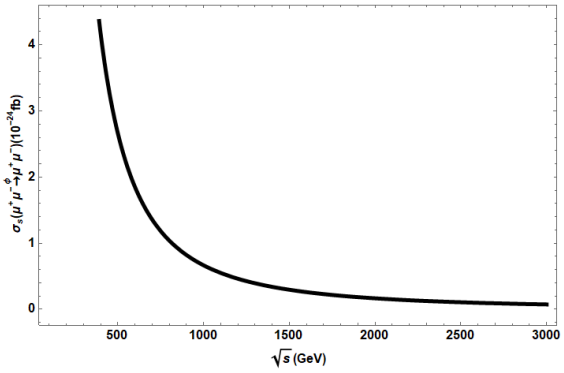

(c) Total cross section as functions of the collision energy via ϕ exchange in s-channel.

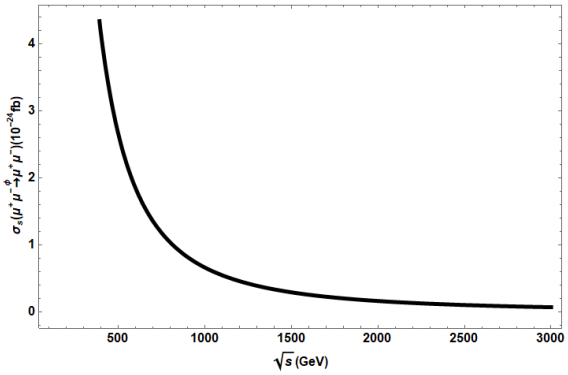

(d) Total cross section as functions of the collision energy via ϕ exchange in t-channel.

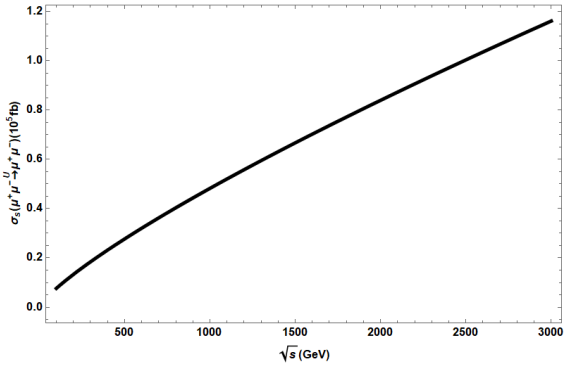

(e) Total cross section as functions of the collision energy via *U* exchange in s-channel.

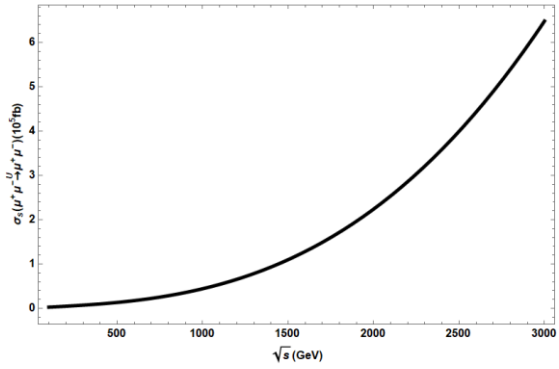

(f) Total cross section as functions of the collision energy via *U* exchange in t-channel.

Figure 7. Total cross sections as functions of the center-of-mass energy via (h, ϕ , U) exchange through two channels s and t.

4. Conclusion

We have done numerical calculations and plotted the cross sections as functions of the scattering angle and the collision energy. As for the scattering angle, the final state should be detected the most via Z, U^{μ}, U exchange. The process via (γ , Z, U^{μ}) exchange, the contribution of Z boson and unparticles are the greatest in t-channel, when cosθ is close to 0.9-1 domain, especially in a very high energy region. In the meantime, the γ and part of Z exchange dominate the lower energy region as cosθ = – 1. The contribution of scalar unparticle in t-channel is more substantial than the other two exchanges (h, ϕ) which only contribute to a slight extent. The results for total cross sections show that the contribution of both scalar and vector unparticle exchange dominates in the very high energy region, while γ has made the major contribution in the lower energy, below 1 TeV. Z boson also contributes greatly to the final state observation in the region of 1,5 - 3 TeV, however less significant than the unparticle. Higgs-radion mixing only makes the extremely small contribution in the whole process, specifically in the whole range of high energy. More importantly, unparticle physics matters in new energy frontiers and high energy reach of colliders generally. The measurements and observation for new physics and other important processes therefore become more physically recognizable in the upcoming valid experiments.

References

[1] T. Banks, A. Zaks, On the Phase Structure of Vector-like Gauge Theories With Massless Fermions, Nucl. Phys. B196, Vol. 196, No. 2, 1982, pp. 189-204.

[2] H. Georgi, Unparticle Physics, Phys. Rev. Lett. 98 221601, Vol. 98, No. 22, 2007, https://doi.org/10.1103/physrevlett.98.221601.

[3] H. Georgi, Another Odd Thing About Unparticle Physics, Phys. Rev. Lett. B, Vol. 650, No. 4, 2007, pp. 275-278 https://doi.org/10.48550/arXiv.0704.2457.

[4] S. Coleman, E. Weinberg, Radiative Corrections as the Origin of Spontaneous Symmetry Breaking, Phys. Rev. D **7**, Vol. 7, Iss. 6, 1973, pp. 1888-1910, https://doi.org/10.1103/PhysRevD.7.1888.

[5] K. Cheung, W. Y. Keung, T. C. Yuan, Collider Phenomenology of Unparticle Physics, Phys. Rev. D 76, Vol. 76, No. 5, 2007, https://doi.org/10.1103/PhysRevD.76.055003.

[6] S. L. Chen, X. G. He, Interactions of Unparticles with Standard Model Particles, Phys. Rev. D 76, Vol. 76, No. 9, 2007, https://doi.org/10.1103/PhysRevD.76.091702.

[7] L. Randall, R. Sundrum, Large Mass Hierarchy from A Small Extra Dimension, Phys. Rev. Lett. 83, Vol. 83, No. 17, 1999, pp. 3370-3373, https://doi.org/10.1103/physrevlett.83.3370.

[8] J. P. Delahaye, M. Diemoz, K. Long, B. Mansouli´e, N. Pastrone, L. Rivkin, D. Schulte, A. Skrinsky, A. Wulzer, Muon Colliders, European Particle Physics Strategy Update by the Muon Collider Working Group, 2019, arXiv:1901.06150 [physics.acc-ph].

[9] D. Stratakis et al., A Muon Collider Facility for Physics Discovery, Proceedings of Snowmass'21, 2022, https://arxiv.org/abs/2203.08033.

[10] K. Long, D. Lucchesi, M. Palmer, N. Pastrone, D. Schulte, V. Shiltsev, Muon Colliders: Opening New Horizons for Particle Physics, Vol. 17, No. 3, 2021, pp. 282-292, https://doi.org/10.48550/arXiv.2007.15684.

[11] M. E. Peskin, D. V. Schroeder, An Introduction to Quantum Field Theory, Addision-Wesley Publishing, 2018.

[12] D. Dominici, B. Grzadkowski, J. F. Gunion, M. Toharia, The Scalar Sector of The Randall–Sundrum Model, Nucl. Phys. B671, Vol. 671, 2003, pp. 243-292, https://doi.org/10.1016/j.nuclphysb.2003.08.020.

[13] D. V. Soa, D. T. L. Thuy, N. H. Thao, T. D. Tham, Radion Production in γe- Collisions, Mod. Phys. Lett. A27, Vol. 27, No. 23, 2012, https://doi.org/10.1142/S021773231250126X.

[14] J. D. Blas et al., The Physics Case of A 3 TeV Muon Collider Stage, 2022, https://doi.org/10.48550/arXiv.2203.07261.

[15] S. Jindariani et al., Promising Technologies and R&D Directions for the Future Muon Collider Detectors, 2022, https://doi.org/10.48550/arXiv.2203.07224.

[16] C. Aime et al., Muon Collider Physics Summary, High Energy Physics - Phenomenology (hep-ph), High Energy Physics - Experiment (hep-ex), FOS: Physical Sciences, 2022,, https://doi.org/10.48550/arXiv.2203.07256.

[17] D. Neuffer, V. Shiltsev, on the Feasibility of A Pulsed 14 TeV C.m.e. Muon Collider in the LHC Tunnel, Journal of Instrumentation, Vol. 13, No. 10, 2018, pp. 10003, https://doi.org/10.1088/1748-0221/13/10/t10003.

[18] V. D. Shiltsev, High-energy Particle Colliders: Past 20 Years, Next 20 Years and Beyond, Physics-Uspekhi Vol. 55, No. 10, 2012, pp. 965-976, https://doi.org/10.48550/arXiv.1409.5464.